

pubs.acs.org/Macromolecules Article

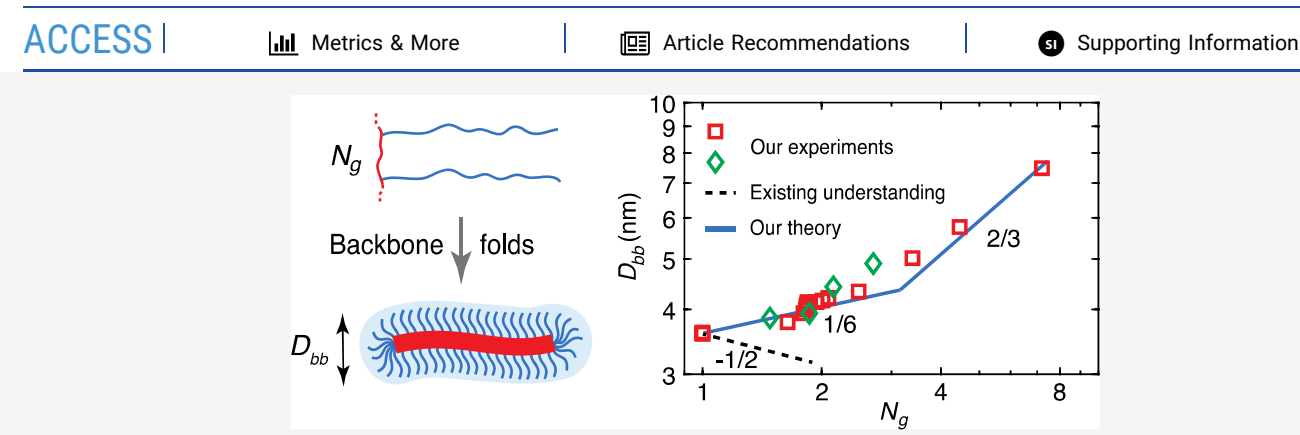
Unexpected Folding of Bottlebrush Polymers in Melts

Shifeng Nian, Baiqiang Huang, Guillaume Freychet, Mikhail Zhernenkov, and Li-Heng Cai*



Cite This: Macromolecules 2023, 56, 2551-2559





ABSTRACT: Bottlebrush molecules are branched polymers with a long linear backbone densely grafted by many relatively short linear side chains. Such a unique molecular architecture enables bottlebrush polymers with properties and functions inaccessible by their linear counterparts. The existing understanding is that, in melts of bottlebrush polymers, the interbackbone distance decreases as the grafting density of side chains becomes smaller. Here, we experimentally discover a behavior opposite to all existing works: the interbackbone distance increases monotonically as the grafting density decreases. To explain these remarkable experimental findings, we develop a theory by accounting for the incompatibility between the backbone and side chains within a bottlebrush molecule. The backbone polymer folds into a cylindrical core with all grafting sites on its surface to reduce interfacial free energy. As the grafting density decreases, the backbone collapses; this process not only increases the diameter of the cylindrical core but also reduces the distance between grafting sites in space, such that the extension of side chains is not alleviated. Our discovery presents a paradigm-shifting understanding of the molecular structure of bottlebrush polymers.

1. INTRODUCTION

Bottlebrush molecules are branched polymers with a long linear backbone densely grafted by many relatively short linear side chains. Such a unique molecular architecture enables bottlebrush polymers with properties and functions inaccessible by their linear counterparts. In nature, bottlebrush biopolymers such as mucins and aggrecans are critical to many biological functions such as lubricin for joints, 1-5 protective mucosal barriers, 6,7 and signaling in malignant cells. 8 As an individual molecule, the chemical species of constituent components of a bottlebrush polymer can be tailored through modern synthesis techniques. 9,10 This versatility offers a wide range of parameter space to design molecules for various applications such as drug carriers 11 and contrast agents for in vivo imaging. 12 As basic building blocks of a material collective, bottlebrush molecules can be tuned in size from nanometers 13,14 to micrometers 15 to create structures with mesoscale characteristic lengths and multiscale ordering, enabling polymeric materials of fascinating rheological, mechanical, optical, and/or dielectric properties. 16-22 Examples include bottlebrush polymer-based super lubricants, 23 adhesives, 24 photonic crystals, 25 and, very recently, extremely soft yet solvent-free elastomers with stiffnesses matching that of hydrogels and "watery" biological tissues.^{26–33} Nevertheless, as for any polymers, it is of foundational importance to understand the molecular structure of bottlebrush polymers.

The existing understanding is that the steric repulsion among the highly overlapping side chains extends the backbone of a bottlebrush polymer. At very high grafting density, the side chains stretch radially away from the backbone polymer to avoid crowding. Through these processes, the side chains occupy a cylindrical volume centering the contour of the backbone polymer. Thus, analogous to the difference between sausage and spaghetti, a bottlebrush molecule is effectively a "fat" linear polymer with renormalized Kuhn segment size about the bottlebrush diameter. Because the Kuhn segments are space-filling in melts, the bottlebrush diameter almost equals the interbackbone distance, $D_{\rm bb}$. Despite some debate on the exact

Received: October 4, 2022 Revised: December 17, 2022 Published: January 27, 2023





dependence of $D_{\rm bb}$ on the degree polymerization (DP) $N_{\rm sc}$ of a side chain, $D_{\rm bb} \propto N_{\rm sc}^{\alpha}$ in which α ranges from 0.35 to 0.5 depending on the length of the side chain, $^{34-36}$ it is widely accepted that $D_{\underline{b}\underline{b}}$ decreases as the grafting density of side chains decreases.

Here, we experimentally discover a phenomenon opposite to all existing works: in melts of bottlebrush polymers, D_{bb}increases monotonically with the decrease of side chain grafting density. We design and synthesize bottlebrush polymers with chemically different backbone and side chains; this allows quantifying D_{bb} in bottlebrush polymer melts using X-ray scattering. As the grafting density decreases by nearly 7 times, $D_{\rm bb}$ increases by more than 2 times. This trend is further verified using different polymer species. To explain the remarkable experimental findings, we develop a theory by accounting for the incompatibility between the side chains and the backbone polymer of a bottlebrush. The backbone polymer folds into a cylindrical core with all grafting sites on its surface to reduce interfacial free energy. As the grafting density decreases, the backbone polymer collapses; this process not only increases the diameter of the cylindrical core but also reduces the distance between grafting sites in space, such that extension of side chains is not alleviated. Our discovery presents a paradigm-shifting understanding of the molecular structure of bottlebrush polymers.

2. RESULTS AND DISCUSSION

We consider a bottlebrush polymer consisting of linear side chains spaced by a polymer section with average DP of N_a (Figure 1a). The number of side chains per bottlebrush polymer, $n_{\rm sc}$, is much larger than the DP of the side chain, $n_{\rm sc}$ $\gg N_{\rm sc}$, such that end effects can be ignored. We use l, v, b, and L_{max} respectively, to denote the length of the main-chain bond of a chemical monomer, the volume of a chemical monomer, the length of a Kuhn segment, and the contour length of a linear polymer. We use "sc" and "bb" as subscripts or superscripts to denote the side chains and the backbone, respectively.

We start with summarizing the prevailing understanding of the molecular structure of bottlebrush polymers in melts. In brief, at relatively low grafting density when the side chains are far apart from each other, the side chain adopts an unperturbed Gaussian conformation. The mean-square end-to-end distance of an unperturbed side chain is

$$R_{\rm sc,0}^2 \approx b_{\rm sc} L_{\rm max}^{\rm sc} \approx b_{\rm sc} l_{\rm sc} N_{\rm sc} \tag{1}$$

As the grafting density increases or $N_{\rm g}$ becomes smaller, the side chains from the same bottlebrush polymer can overlap. Yet, they will not completely fill the volume pervaded by one side chain of unperturbed size, $V_{\rm P} \approx R_{\rm sc,0}^3$, until a crossover grafting density $1/N_g^*$

$$R_{\rm sc,0}^3 \approx N_{\rm sc} v_{\rm sc} \left(\frac{g}{N_{\rm g}^*} \right)$$
 (2)

Here, g is the number of monomers in a backbone section passing through the pervaded volume, and g/N_g^* corresponds to the number of side chains within V_p . At N_g^* , the side chains are not crowded and there is no steric repulsion among the side chains. Thus, the backbone polymer is not extended and adopts an unperturbed Gaussian conformation. Because the

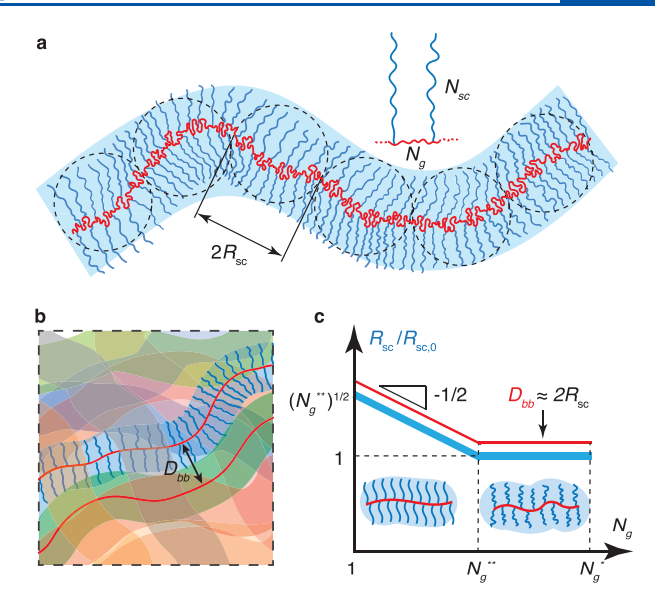


Figure 1. Existing understanding of the molecular structure of bottlebrush polymers in melts. (a) Schematic of a bottlebrush polymer: N_{sc} DP of a side chain; N_{g} average DP of the backbone section between two neighboring grafting sites. A bottlebrush molecule is effectively a "fat" linear polymer with a diameter about twice the root-mean-square end-to-end distance of a side chain, $R_{\rm sc}$ (b) In the melt of bottlebrush polymers, the average distance D_{bb} between the backbones of two neighboring bottlebrush molecules is about the bottlebrush diameter (thin red line). (c) The prevailing understanding is that R_{sc} decreases with the increase of N_g by a power of -1/2 up to N_g^{**} [eq 5], above which the side chain adopts an unperturbed Gaussian conformation with the size of $R_{sc,0}$ [eq 1] (thick blue line). For $N_{\rm g}$ < $N_{\rm g}^*$ [eq 3], the side chains from the same bottlebrush completely fill the cylindrical space surrounding the bottlebrush backbone; thus, the interbackbone distance is about twice the side chain size $D_{\rm bb} \approx 2R_{\rm sc}$ (red line) [eq 6].

size of the backbone section with g monomers is about that of

the side chain,
$$(gl_{bb}b_{bb})^{1/2} \approx R_{sc,0}$$
, eq 2 can be rewritten as
$$N_{\rm g}^* \approx N_{\rm sc}^{1/2} \frac{v_{\rm sc}}{\left(b_{\rm sc}l_{\rm sc}\right)^{1/2} \left(l_{bb}b_{bb}\right)} \tag{3}$$

As the grafting density further increases with $N_{\rm g} < N_{\rm g}^*$, the space near the backbone polymer is not enough to accommodate all the side chains from the same bottlebrush if the backbone remains in an unperturbed Gaussian conformation. To avoid the crowding of side chains, the backbone polymer must extend. This process ensures a constant distance in space between two neighboring grafting sites. In doing so, the side chains remain in an unperturbed Gaussian conformation of size $R_{sc,0}$ [eq 1]. By contrast, the backbone polymer continues to extend as the grafting density increases. However, the extension of the backbone cannot continue forever; instead, it will stop at certain grafting density N_{σ}^{**} , at which the backbone section between two neighboring grafting sites is stretched to its maximum contour length.

At high grafting density with $1 < N_g < N_g^{**}$, there is no other way for the side chains to avoid crowding except by radially extending away from the backbone polymer. An intuitive way to appreciate this physical picture is by considering such a densely grafted bottlebrush molecule as a "fat" linear polymer with a cross-section about twice the side chain size, as illustrated in Figure 1b. The side chain size R_{sc} is determined by volume conservation: a side chain of volume $v_{sc}N_{sc}$ fills the

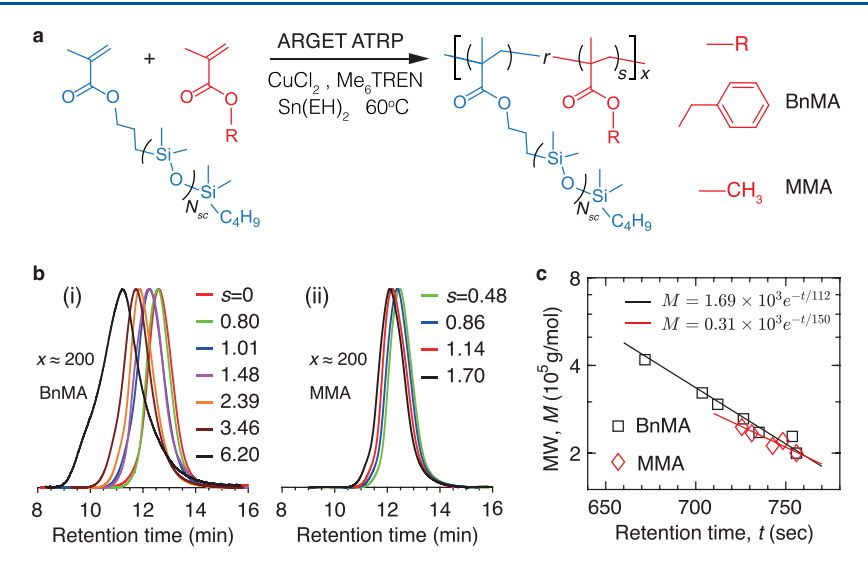


Figure 2. Design and synthesis of bottlebrush polymers with controlled grafting density. (a) A bottlebrush polymer is synthesized by copolymerizing methacrylate-terminated PDMS with an MW of 1000 g/mol and BnMA with an MW of 176 g/mol or methyl methacrylate (MMA) with an MW of 100 g/mol. x, the number of side chains per bottlebrush molecule; s: the molar ratio between the side chains and spacer monomers. (b) GPC traces of bottlebrush polymers with (i) BnMA and (ii) MMA as spacers. (c) The logarithmic MW, M, of all bottlebrush polymers decreases linearly with the increase of peak retention time, t.

cylindrical space $R_{\rm sc}^2 N_{\rm g} l_{\rm bb}$ surrounding the backbone polymer: $R_{\rm sc}^2 N_{\rm g} l_{\rm bb} \approx \nu_{\rm sc} N_{\rm sc}$. This gives

$$R_{\rm sc} \approx \left(\frac{\nu_{\rm sc} N_{\rm sc}}{N_{\rm g} l_{\rm bb}}\right)^{1/2} \approx R_{\rm sc,0} \left(\frac{N_{\rm g}^{**}}{N_{\rm g}}\right)^{1/2},$$
for $1 < N_{\rm g} < N_{\rm g}^{**}$ (4)

As a result, the side chain size decreases with the increase of $N_{\rm g}$ by a power of -1/2 (blue line, Figure 1c). Also, $1/N_{\rm g}^{**}$ is the crossover grafting density above which the side chains start to extend:

$$N_{\rm g}^{**} \approx \frac{\nu_{\rm sc}}{b_{\rm sc}l_{\rm sb}} \tag{5}$$

The above understanding for bottlebrush polymers in melts can be summarized into two widely accepted physical pictures. First, for $N_{\rm g} < N_{\rm g}^*$, the bottlebrush is reminiscent of a filament with a diameter about twice the side chain size. Second, the bottlebrush diameter is a constant at intermediate high grafting density with $N_{\rm g}^* > N_{\rm g} > N_{\rm g}^{**}$; whereas at very high grafting density with $N_{\rm g} < N_{\rm g}^{**}$, the diameter increases with grafting density $1/N_{\rm g}$ by a power of 1/2. This understanding has been pointed out in pioneering experimental works, 26,27 confirmed by simulations, 36 and detailed in a seminal work by Rubinstein Lab; 37 however, this has never been rigorously tested by experiments.

We seek to experimentally quantify the diameter of a bottlebrush polymer in melts. Yet, this is extremely difficult because of limited contrast between an individual bottlebrush polymer and the surrounding environment. In addition, the diameter of a typical bottlebrush polymer is less than 10 nm. Thus, the difference in bottlebrush diameter attributed to the change in grafting density, if any, is on the order of subnanometers. Moreover, because of thermal fluctuations, the diameter of the bottlebrush fluctuates. These pose additional challenges in precisely measuring the effects of grafting density on the bottlebrush diameter using optical imaging techniques.³⁸

Alternatively, the interbackbone distance $D_{\rm bb}$ for bottlebrush polymers in a melt is about the bottlebrush diameter, as schematically illustrated in Figure 1b and shown by the red line in Figure 1c.

$$D_{\rm bb} = \lambda \beta^{1/2} (2R_{\rm sc}) \propto \begin{cases} \left(\frac{N_{\rm g}^{**}}{N_{\rm g}}\right)^{1/2}, & \text{for } 1 < N_{\rm g} < N_{\rm g}^{**} \\ 1, & \text{for } N_{\rm g}^{**} < N_{\rm g} < N_{\rm g}^{*} \end{cases}$$
(6)

Here, $\beta=0.78$ is the fraction of the area covered by hard disks randomly packed in two-dimensional space, and λ is a scaling prefactor on the order of unity. Moreover, instead of using deuterated polymers to create a contrast for neutron scattering, it is possible to exploit the chemically different backbone polymer and side chains to achieve a contrast in electron density; this would allow direct measurement of $D_{\rm bb}$ using relatively widely accessible X-ray scattering. ^{28,32,39,40} Thus, quantifying $D_{\rm bb}$ provides an alternative approach to measuring the diameter of a bottlebrush polymer in melts.

We design a bottlebrush using methacrylate-based backbone polymer and linear poly(dimethyl siloxane) (PDMS) as side chains. In the melt of such bottlebrush polymers, the backbone—backbone distance can be unambiguously resolved by wide-angle X-ray scattering (WAXS), as demonstrated in our previous studies.³² We denote a bottlebrush polymer as (MASP_s-r-PDMS^y)_{xy} in which $x = n_{sc}$ is the number of PDMS side chains, y = 1 is the molecular weight (MW) of PDMS in kg/mol, and s is the molar ratio between the methacrylate-based spacer monomer (MASP) and linear PDMS side chains. We keep N_g smaller than the DP per Kuhn segment N_k for the methacrylate-based polymer to ensure a relatively high grafting density (Supporting Information Text).

Guided by the above design, we synthesize bottlebrush molecules by copolymerizing methacrylate-terminated PDMS (MA-PDMS) and benzyl methacrylate (BnMA) using our previously developed procedure ^{29,30,32,41} (Figure 2a). The

method is based on activator-regenerated-by-electron-transfer atom-transfer radical polymerization, in which catalysts are constantly regenerated from reducing organic reagents; 42 this improves the tolerance to oxygen and significantly reduces the required catalyst concentration, enabling controlled synthesis of large bottlebrush polymers. We fix the number of side chains at $n_{\rm sc} \approx 200$ while increasing the fraction of spacers s from 0 to 6.2, corresponding to $N_g = s + 1$ from 1 to 7.2. For the synthesis of each polymer, we use slightly different reaction conditions and stop the reaction at a conversion in the range of 30-45% (Tables S2 and S3), in which the reaction rates of the side chain and spacer monomer are nearly the same (Figure S1). This approach avoids the formation of blocky or gradient bottlebrush polymers and ensures that the side chains are randomly spaced by spacer monomers. The success of the synthesis is confirmed by proton nuclear magnetic resonance (¹H NMR) spectroscopy (Supporting Information). The purified polymers are further characterized by gel permeation chromatography (GPC) (Figure 2b(i)), based on which the polydispersity index (PDI) is determined to be about 1.2 (Table 1). The peak retention time decreases as the fraction of

Table 1. Molecular Parameters of Bottlebrush Polymers^a

	bottlebrush polymers					WAXS	
sample	spacer	$n_{\rm sc}$	$n_{\rm sp}$	s	PDI	$\binom{q_{\mathrm{bb}}}{(\mathrm{nm}^{-1})}$	$D_{ m bb} \ m (nm)$
S_1	BnMA	205	0	0	1.24	1.75	3.59
S_2		195	125	0.64	1.26	1.66	3.78
S_3		200	160	0.80	1.22	1.6	3.93
S_4		200	202	1.01	1.25	1.51	4.16
S_5		206	305	1.48	1.31	1.45	4.33
S_6		207	495	2.39	1.35	1.25	5.02
S_7		200	692	3.46	1.48	1.09	5.76
S_8		198	1228	6.20	1.98	0.84	7.48
S_9		306	254	0.83	1.37	1.57	4.00
S_{10}		402	338	0.84	1.41	1.54	4.08
S_{11}		508	422	0.83	1.48	1.55	4.05
S_{12}		534	448	0.84	1.44	1.52	4.13
S ₁₃		378	0	0	1.33	1.74	3.61
S_{14}		468	440	0.94	1.44	1.52	4.13
S ₁₅		360	389	1.08	1.40	1.49	4.21
S ₁₆	MMA	210	101	0.48	1.23	1.63	3.85
S ₁₇		195	168	0.86	1.37	1.60	3.93
S_{18}		210	239	1.14	1.31	1.42	4.42
S_{19}		210	357	1.70	1.38	1.28	4.90

 $^an_{\rm sc}$, number of PDMS side chains per bottlebrush; $n_{\rm sp}$, number of spacer monomers per bottlebrush; s: molar ratio between the side chains and spacer monomers per bottlebrush; PDI, polydispersity index; $q_{\rm bb}$, wavenumber of the characteristic scattering peak; and $D_{\rm bb}=2\pi/q_{\rm bb}$, interbackbone distance.

spacer monomers s increases (Figure 2b(i)). As expected, the MW, M, determined from NMR decreases logarithmically with the increase of peak retention time, t (black solid line and squares in Figure 2b). These results confirm the accuracy of $n_{\rm sc}$ and s determined by NMR. Because s is the only variable, these polymers provide an ideal system for exploring the dependence of $D_{\rm bb}$ on grafting density.

We use synchrotron source to perform WAXS measurements for melts of bottlebrush polymers. In a typical measurement, we predissolve the polymer in dichloromethane, load the solution into a quartz glass capillary, and evaporate the

solvent in a vacuum oven at 25 °C to leave a polymer melt (Experimental Section). We measure at multiple locations to ensure the consistency of two-dimensional (2D) WAXS patterns, as exemplified in Figure 3a(i). By subtracting the background from the glass capillary and radially average the 2D patterns, we obtain the one-dimensional (1D) scattering intensity I as a function of the absolute value of the scattering wavevector q, as shown in Figure 3a(ii). All polymers exhibit only one pronounced characteristic peak $q_{\rm bb}$, which is associated with the interbackbone distance by $D_{\rm bb} = 2\pi/q_{\rm bb}$.

The interbackbone distance for the melt of bottlebrush polymer with the highest grafting ($N_{\rm g}=1$) is 3.59 nm (red arrow in Figure 3a(ii) and Table 1). This value agrees with that reported by another laboratory for the same bottlebrush polymer. Moreover, the experimentally measured value agrees well with the theoretical prediction: $D_{\rm bb}=\lambda\beta^{1/2}(2R_{\rm sc})$ [eq 6], in which $\lambda=0.76$ is the scaling perfector and $R_{\rm sc}\approx \left(\frac{v_{\rm sc}N_{\rm sc}}{l_{\rm bb}N_{\rm g}}\right)^{1/2}\approx 2.6$ nm. Here, $v_{\rm sc}=127~{\rm \AA}^3$ is

the volume of a PDMS chemical monomer, $N_{\rm sc} \approx 14$, and $l_{\rm bb} = 2.56$ Å is main C–C chain length of the backbone (see Table S1, Supporting Information Text). These results confirm that the bottlebrush diameter can be measured as $D_{\rm bb}$.

The bottlebrush diameter $D_{\rm bb}$ is independent of the number of side chains per bottlebrush. For example, at $N_{\rm g}=1$, as $n_{\rm sc}$ increases by nearly twice from 200 to ~400, the location of $q_{\rm bb}$ remains the same (Figure S2). Similar behavior is observed for a lower grafting density with $N_{\rm g}=1.83$ but various $n_{\rm sc}$ ranging from 200 to 500, as shown by nearly the same $q_{\rm bb}$ location in Figure 3a(iii). This behavior further confirms the synthesis of bottlebrush polymers with nearly randomly grafted side chains, which would otherwise result in blocky or gradient bottlebrush polymers forming domains with size increasing with the polymer MW.

Remarkably, $D_{\rm bb}$ increases monotonically with the decrease of grafting density, as evidenced by the shift of $q_{\rm bb}$ toward lower values at higher $N_{\rm g}$ (Figure 3a(ii)). Moreover, as $N_{\rm g}$ increases by more than 7 times from 1 to 7.2, $D_{\rm bb}$ increases, not decreases, by more than 2 times from 3.59 to 7.48 nm. This behavior is opposite to the existing understanding that $D_{\rm bb}$ decreases with the increase of $N_{\rm g}$ [eq 6] (red line, Figure 1c).

To test whether the observed behavior is specific to the BnMA-spaced PDMS bottlebrush, we synthesize an additional series of bottlebrush polymers using methyl methacrylate (MMA) as the spacer monomer [Figure 2b(ii) and diamonds in Figure 2c]. Compared to BnMA of 176 g/mol, MMA has a lower MW of 100 g/mol but has the same methacrylate group, such that $D_{\rm bb}$ can be resolved using WAXS (Figure 3b). Remarkably, a similar trend is observed: $D_{\rm bb}$ increases with the increase of $N_{\rm g}$ (green diamonds in Figure 4a). This behavior is opposite to the existing understanding (dashed line in Figure 4a). Such a qualitative disagreement strongly indicates that the classical understanding of bottlebrush polymers is incomplete.

We note that existing understanding assumes the backbone polymer and the side chains to be compatible.³⁷ However, that is not the case in most experiments including ours, where the backbone polymer and the side chains are of different chemical species. Indeed, the methacrylate-based backbone and the PDMS side chains are highly incompatible with the Flory—Huggins interaction parameter $\chi \approx 0.2$.⁴³ Thus, a bottlebrush polymer is reminiscent of a copolymer, in which the backbone polymer is prone to phase separate from the side chains to

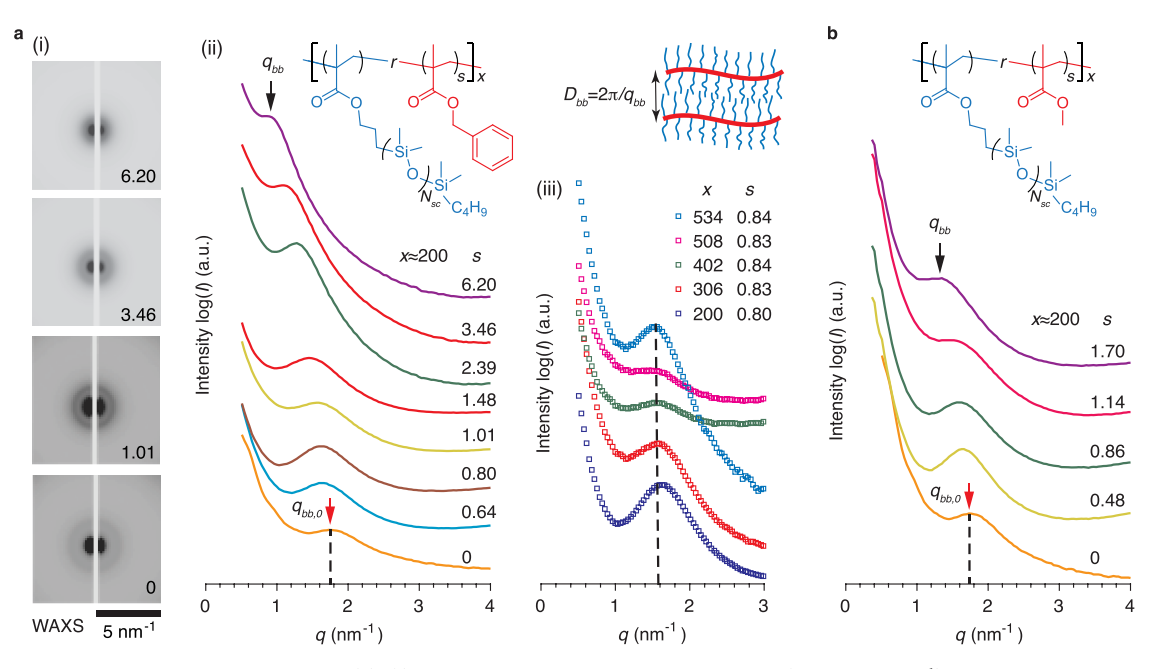


Figure 3. WAXS of bottlebrush polymer melts. (a) (i) Representative 2D WAXS patterns for $(BnMA_s - PDMS^1)_x$ bottlebrush polymers with $x \approx 200$. (ii,iii) Radially averaged 1D scattering intensity I as a function of the magnitude of the wavevector q for various bottlebrush polymers with BnMA as spacer monomers: (ii) fixed $x \approx 200$ but various s; (iii) fixed $s \approx 0.83$ but various s. a.u., arbitrary units. (b) Melts of bottlebrush polymers with MMA as spacer monomers. q_{bb} , wavenumber of the characteristic peak; $D_{bb} = 2\pi/q_{bb}$, interbackbone distance.

reduce interfacial free energy. However, unlike a binary mixture consisting of incompatible molecules such as water and oil, where the minority phase tends to form spherical droplets with minimized surface area, the microphase separation within the grafted polymer is constrained by chain connectivity. Thus, instead of forming a spherical domain, the backbone polymer can fold into a cylindrical core with all grafting sites on its surface (inset, Figure 4b).

Based on above arguments, we extend the theory by Rubinstein Lab³⁷ to a more general scenario where the side chains and the backbone of bottlebrush are incompatible. We focus on the strongly segregated case where the interface between distinct domains is sharp. This condition requires all the grafting sites to be at the surface, not in the interior, of the cylindrical core folded by the backbone polymer. Yet, in our experiments $N_{\rm g} \leq 7.2 < N_{\rm k,bb}$, in which $N_{\rm k,bb} = 7.3$ is the number of chemical monomers per Kuhn segment for PBnMA (Table S1). Thus, the diameter of the cylinder must be smaller than the Kuhn length $b_{\rm bb}$ = 1.86 nm of PBnMA. Moreover, the Kuhn segment is not spherical but cylindrical with an aspect ratio of 3-5 (Supporting Information Text). Thus, the only way that the backbone polymer can pack in such a slim cylinder is by stacking Kuhn segments along the contour of the cylinder. This phenomenon is reminiscent of filling a long tube with a chain of cylindrical particles longer than the tube diameter, as illustrated in Figure 4b. In doing so, all grafting sites are at the surface rather than in the interior of the cylinder to reduce interfacial free energy.

To calculate the diameter of the bottlebrush, we consider the free energy of a folded bottlebrush polymer. The steric repulsion among the strongly overlapping side chains tends to elongate the cylindrical core. By contrast, the backbone polymer tends to collapse to a cylinder of a larger diameter, such that the interfacial area between the side chains and the backbone polymer can be reduced. Thus, the total free energy $F_{\rm tot}$ of a bottlebrush polymer is

$$F_{\text{tot}} = F_{\text{sc}} + F_{\text{bb}} + F_{\text{int}} \approx F_{\text{sc}} + F_{\text{int}} \tag{7}$$

where $F_{\rm int}$ is the interfacial free energy between the incompatible backbone and side chains, and $F_{\rm sc}$ and $F_{\rm bb}$ are, respectively, the entropic free energies due to the stretching of the side chains and the backbone polymer. However, $F_{\rm bb}$ can be ignored because the stretching of the backbone polymer is comparable to that of one side chain (see the Supporting Information Text),³⁷ and there are many side chains per bottlebrush polymer.

The interfacial free energy between the side chains and the backbone polymer is

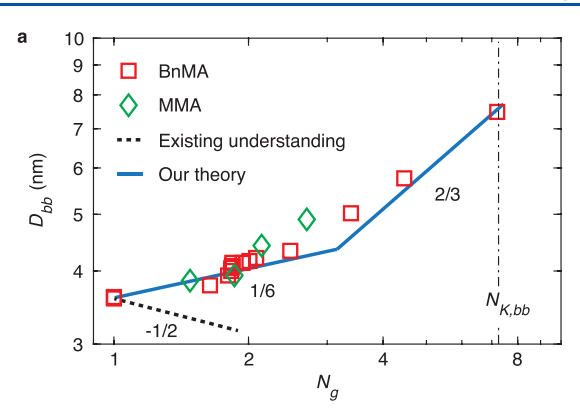
$$\frac{F_{\rm int}}{k_{\rm B}T} \approx r_{\rm c} L_{\rm c} \left(\frac{\chi}{a_0}\right) \tag{8}$$

Here, $r_c L_c$ is the total surface area of the cylindrical core, and χ/a_0 is the interfacial free energy per contact area a_0 of a Kuhn segment. The length L_c of the cylinder is given by the volume conservation of the backbone polymer: $n_{\rm sc}N_{\rm g}\nu_{\rm bb}\approx r_{\rm c}^2L_{\rm c}$. Thus, eq 8 can be rewritten as

$$\frac{F_{\rm int}}{k_{\rm B}T} \approx \left(\frac{\chi}{a_0}\right) \frac{n_{\rm sc} N_{\rm g} \nu_{\rm bb}}{r_{\rm c}} \tag{9}$$

To calculate the entropic free energy of side chains, we consider a section of the cylindrical core with the length of $b_{\rm bb}$. The number of side chains grafted to this cylindrical section is $b_{\rm bb} r_{\rm c}^2/(N_{\rm g} v_{\rm bb})$, in which $b_{\rm bb} r_{\rm c}^2$ is the volume of the section of the cylindrical core, and $N_{\rm g} v_{\rm bb}$ is the volume of the backbone section between two neighboring grafting sites. Surrounding the cylindrical core, these side chains fill the space with a volume of $[(R_{\rm sc} + r_{\rm c})^2 - r_{\rm c}^2]b_{\rm bb}$; this gives

$$[(R_{\rm sc} + r_{\rm c})^2 - r_{\rm c}^2]b_{\rm bb} \approx \frac{b_{\rm bb}r_{\rm c}^2}{N_{\rm g}\nu_{\rm bb}}N_{\rm sc}\nu_{\rm sc}$$
(10)



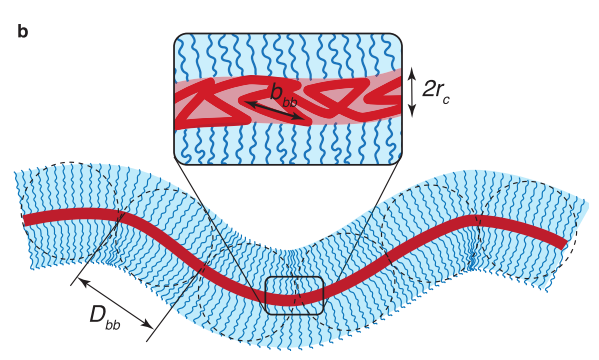


Figure 4. Bottlebrush polymers fold in melts. (a) The interbackbone distance, $D_{\rm bb}$, increases with the decrease of grafting density, $1/N_{\rm g}$. The bottlebrush polymers consist of linear PDMS side chains spaced by BnMA (red squares) and MMA (green diamonds) monomers (Table 1). Dashed line: prediction of existing theory [eq 6]; solid line: prediction of our theory [eq 17]. $N_{\rm K,bb}$, DP of the Kuhn segment of PBnMA. (b) A schematic for the molecular structure of bottlebrush polymers in melts by accounting for the incompatibility between side chains (blue lines) and the bottlebrush backbone (red lines). The backbone folds to a cylindrical core with a radius r_{c} , and the Kuhn segments of length $b_{\rm bb}$ are packed along the cylindrical core with all grafting sites on its surface (inset, b). The shadowed region indicates the volume occupied by the side chains from the same bottlebrush polymer.

Assuming that the side chain size is much larger than the diameter of the cylindrical core, $R_{\rm sc} \gg r_{\rm c}$ the effects of cylindrical core on the volume available to the side chains can be neglected

$$(R_{\rm sc} + r_{\rm c})^2 - r_{\rm c}^2 \approx R_{\rm sc}^2$$
, for $R_{\rm sc} \gg r_{\rm c}$ (11)

Rewriting eq 10 gives the side chain size

$$R_{\rm sc} \approx r_{\rm c} \left(\frac{N_{\rm sc} \nu_{\rm sc}}{N_{\rm g} \nu_{\rm bb}}\right)^{1/2}$$
, for $R_{\rm sc} \gg r_{\rm c}$ (12)

The entropic free energy due to the stretching of $n_{\rm sc}$ side chains of the bottlebrush polymer is

$$\frac{F_{\rm ent}}{k_{\rm B}T} \approx n_{\rm sc} \left(\frac{R_{\rm sc}}{R_{\rm sc,0}}\right)^2 \approx n_{\rm sc} r_{\rm c}^2 \frac{\nu_{\rm sc}}{N_{\rm g} \nu_{\rm bb} b_{\rm sc} l_{\rm sc}}$$
(13)

Using eqs 7, 9, and 13, one obtains the total free energy of the bottlebrush polymer

$$\frac{F_{\text{tot}}}{k_{\text{B}}T} = \frac{F_{\text{ent}}}{k_{\text{B}}T} + \frac{F_{\text{int}}}{k_{\text{B}}T} \approx \left(\frac{\chi}{a_0}\right) \frac{n_{\text{sc}}N_{\text{g}}\nu_{\text{bb}}}{r_{\text{c}}} + n_{\text{sc}}r_{\text{c}}^2 \frac{\nu_{\text{sc}}}{N_{\text{g}}\nu_{\text{bb}}b_{\text{sc}}l_{\text{sc}}}$$
(14)

Minimizing the total free energy gives the equilibrium crosssectional size of the cylindrical core

$$r_{\rm c,e} \approx \left(\frac{\chi}{a_0}\right)^{1/3} \left(\frac{\nu_{\rm bb}^2 b_{\rm sc} l_{\rm sc}}{\nu_{\rm sc}}\right)^{1/3} N_{\rm g}^{2/3} \equiv r_0 N_{\rm g}^{2/3}$$
 (15)

in which $r_0 \equiv \left(\frac{\chi}{a_0}\right)^{1/3} \left(\frac{v_{bb}^2 b_{sc} l_{sc}}{v_{sc}}\right)^{1/3}$ is a length scale determined

by the Flory–Huggins interaction parameter χ . Substituting eq 15 into eq 12 gives the equilibrium size of the side chain

$$R_{\rm sc,e} \approx r_{\rm c,e} \left(\frac{N_{\rm sc} \nu_{\rm sc}}{N_{\rm g} \nu_{\rm bb}}\right)^{1/2} \approx r_0 \left(\frac{\nu_{\rm sc}}{\nu_{\rm bb}}\right)^{1/2} N_{\rm sc}^{1/2} N_{\rm g}^{1/6}, \text{ for } 1 < N_{\rm g}$$
 $< N_{\rm k,bb}$ (16)

Consequently, the backbone—backbone distance becomes [eqs 15 and 16]

$$D_{bb} \approx R_{sc,e} + r_{c,e} \approx r_0 \left[\left(\frac{\nu_{sc}}{\nu_{bb}} \right)^{1/2} N_{sc}^{1/2} N_g^{1/6} + N_g^{2/3} \right],$$
for $1 < N_g < N_{k,bb}$ (17)

Expression 17 predicts that the interbackbone distance $D_{\rm bb}$ increases with $N_{\rm g}$ Moreover, at very high grafting density (small $N_{\rm g}$) or with long side chains (large $N_{\rm sc}$), the $D_{\rm bb}$ scales with $N_{\rm g}$ by a power of 1/6: $D_{\rm bb} \sim N_{\rm g}^{1/6}$. However, the window for this regime is very small because the diameter of the cylindrical core $r_{\rm c}$ becomes noticeable at relatively large $N_{\rm g}$; this makes the approximation in eq 11 inappropriate. Moreover, the folding of the backbone polymer effectively increases the space available to side chains and thus alleviates the crowding of side chains. Such a correction to the side chain size is beyond the scope of this work and will be the subject of future explorations. Nevertheless, $D_{\rm bb}$ is expected to increase with $N_{\rm g}$ by a power law with an exponent intermediate between 1/6 and 2/3. Indeed, these predications are consistent with our experimental findings, as shown by the solid lines in Figure 4a.

We emphasize that our discovery is qualitatively different from the existing understanding for bottlebrush polymers with compatible ($\chi = 0$) or weakly incompatible side chains and backbone, where the interbackbone distance decreases with $N_{\rm g}$ by a power of -1/2: $D_{\rm bb} \sim N_{\rm g}^{-1/2}$ [eq 4]. Such a remarkable difference originates from the strong segregation between the highly incompatible side chains and backbone polymer, which drives the backbone polymer to fold along its contour. This is possible with the backbone being a flexible polymer, in contrast to bottlebrush polymers with polynorbornene-based backbone, which has a ring structure and is intrinsically stiff.³⁶ The collapse of the backbone polymer further decreases the grafting distance among side chains in space; consequently, this process results in more severe crowding of side chains, such that side chains are more extended. Collectively, the combination of experiments and theory reveals that bottlebrush polymers can fold in melts.

3. CONCLUSIONS

We have designed and synthesized bottlebrush polymers with a wide range of grafting density and the number of side chains. In a bottlebrush polymer, the backbone and the side chains are chemically different; this allows the interbackbone distance of bottlebrush polymers in melts to be precisely measured by WAXS. We discover that the interbackbone distance increases monotonically with the decrease of side chain grafting density. This phenomenon is opposite to all existing works. To explain the remarkable experimental findings, we develop a molecular theory by accounting for the incompatibility between side chains and the backbone polymer. The theory predicts that the backbone polymer folds into a cylindrical core to reduce interfacial free energy. This process increases the sizes of both the backbone domain and the side chains; consequently, the interbackbone distance increases at lower grafting density.

Our findings have important implications in exploiting bottlebrush polymers as building blocks to create responsive structures and functional soft materials. As an individual molecule, a folded bottlebrush polymer is more flexible than rigid nanoparticles and may unfold upon external triggers; these features would enable the folded bottlebrush molecules as responsive nanocarriers that can sneak through complex biological barriers for target drug delivery. 44,45 Compared to conventional bottlebrush polymers, whose backbone is prestrained because of steric repulsions among overlapping side chains,³¹ a folded bottlebrush polymer stores lengths in its collapsed backbone. Because the stored lengths can release upon mechanical stress, crosslinking folded bottlebrush polymers may enable adaptive polymer networks with extreme stretchability. 46 Furthermore, the side chains may be conjugated with functional groups such as reversible bonds to enable unusual dynamic mechanical properties. 47-49 Finally, the concept of foldable bottlebrush polymers is general and could be extended to design bottlebrush-based modular polymeric biomaterials for advanced biomanufacturing. 50,51 Thus, our discovery presents a paradigm-shifting understanding of the molecular structure of bottlebrush polymers, which may stimulate the development of novel soft functional materials.

4. EXPERIMENTAL SECTION

4.1. Materials. Monomethacryloxypropyl-terminated poly-(dimethylsiloxane) (MCR-M11, average molar mass 1000 g/mol) was purchased from Gelest and purified using basic alumina columns to remove inhibitors. BnMA (98%) and MMA (98%) were purchased from Sigma-Aldrich and purified by using basic alumina columns to remove inhibitors. Copper(II) chloride (CuCl₂, 99.999%), tris[2-(dimethylamino)ethyl]amine (Me₆TREN), ethylene bis(2-bromoisobutyrate) (2f-BiB, 97%), tin(II) 2-ethylhexanoate (Sn(EH)₂, 92.5–100%), anisole (\geq 99.7%), and *p*-xylene (\geq 99.7%) were purchased from Sigma-Aldrich and used as received. Tetrahydrofuran [THF, analytical reagent (AR)] was purchased from Macron Fine Chemicals, and THF [high-performance liquid chromatography (HPLC)], methanol (Certified ACS), dichloromethane (Certified ACS), and dimethylformamide (DMF, Certified ACS), were purchased from Fisher, and used as received.

4.2. Polymer Synthesis and Characterization. Despite that the side chain and the spacer monomer have the same methacrylate functional group, their reaction rates could be different. To this end, we use a cosolvent and slightly different reaction conditions for each synthesis, such that the reaction rate of spacer monomers and side chains is nearly the same at conversion up to \sim 45%, as shown in Figure S1. For each synthesis, we stop the reaction at a conversion in the range of 30–45%; this approach ensures a reasonable yield and,

more importantly, bottlebrush polymers with nearly randomly grafted side chains.

The conditions for the synthesis of PDMS bottlebrush polymers with BnMA and MMA spacers are, respectively, detailed in Tables S2 and S3. Also, examples of calculating the molecular parameters of bottlebrush polymers are shown in Figures S4–S7. Here, we use one sample, $(BnMA_{1.01}\text{-PDMS}^1)_{200}$, as an example to describe the procedure for polymer synthesis and characterization.

A 50 mL Schlenk flask is charged with ethylene 2f-BiB (4.3 mg, 0.012 mmol), MCR-M11 (6 g, 6 mmol), BnMA (846 mg, 3.5 mmol), p-xylene (3 mL), and anisole (3 mL). Me₆TREN (92 mg, 0.4 mmol) and CuCl₂ (5.4 mg, 0.04 mmol) are dissolved in 1 mL of DMF to make a catalyst solution. Then, 30 μ L of catalyst solution, containing 0.012 mmol Me₆TREN and 0.0012 mmol CuCl₂, is added to the mixture. The mixture is bubbled with nitrogen for 30 min. After 30 min, $Sn(EH)_2$ (14.6 mg, 0.036 mmol) in 100 μ L of *p*-xylene is quickly dropped into the reaction mixture while bubbling. The flask is then sealed with a rubber stopper and immersed in an oil bath of 60 °C. The conversion of the reaction is monitored by ¹H NMR, and the reaction is stopped at 40% conversion. The reaction mixture is then diluted with THF and passed through a neutral alumina column to remove the catalyst. The collected solution is concentrated using a rotary evaporator (Buchi R-205). The concentrated polymer solution is precipitated in methanol three times to remove unreacted monomers and impurities. After purification, ¹H NMR is used to determine the number of BnMA spacers. For this bottlebrush polymer, it has 202 BnMA spacers and 200 PDMS side chains (s = 1.01) (Figures S4 and S5).

4.3. ¹H NMR Characterization. We use ¹H NMR to determine the number of side chains per bottlebrush and the number of spacer monomers in each bottlebrush polymer. The former one is calculated based on the conversion of PDMS macromonomers to a bottlebrush polymer. The number of spacer monomers is determined based on the NMR spectra of purified bottlebrush polymer (see the Supporting Information, ¹H NMR spectra). Chemical shifts for ¹H NMR spectra are reported in parts per million compared to a singlet at 7.26 ppm in CDCl₂.

4.4. GPC Characterization. GPC measurements are performed using the TOSOH EcoSEC HLC-8320 GPC system with two TOSOH Bioscience TSKgel GMH $_{\rm HR}$ -M 5 μ m columns in series and a refractive index detector at 40 °C. HPLC-grade THF is used as the eluent with a flow rate of 1 mL/min. The samples are dissolved in THF with a concentration around 5 mg/mL. The GPC data of all bottlebrush polymers are shown in Figures 2B and S3. The PDI of all samples are summarized in Table 1.

4.5. WAXS Measurements. We use the soft matter interfaces (12-ID) beamline at the Brookhaven National Laboratory to perform WAXS measurements on bottlebrush polymers. We measure at multiple locations to ensure the consistency of the 2D WAXS patterns. The sample-to-detector distance is 8.3 m, and the radiation wavelength is $\lambda=0.77$ Å. The scattered X-rays are recorded using an in-vacuum Pilatus 300kW detector, consisting of 0.172 mm square pixels in a 941 × 1043 array. The raw WAXS images are converted into q-space, visualized in Xi-CAM software, and radially integrated using a custom Python code. The 1D intensity profile, I(q), is plotted as a function of the scattering wave vector, $|\vec{q}|=q=4\pi\lambda^{-1}\sin(\theta/2)$, where θ is the scattering angle.

ASSOCIATED CONTENT

Supporting Information

The Supporting Information is available free of charge at https://pubs.acs.org/doi/10.1021/acs.macromol.2c02053.

Supporting text, WAXS data, GPC traces, and ¹H NMR spectra (PDF)

AUTHOR INFORMATION

Corresponding Author

Li-Heng Cai — Soft Biomatter Laboratory, Department of Materials Science and Engineering, University of Virginia, Charlottesville, Virginia 22904, United States; Department of Chemical Engineering and Department of Biomedical Engineering, University of Virginia, Charlottesville, Virginia 22904, United States; Orcid.org/0000-0002-6806-0566; Phone: 434-924-2512; Email: liheng.cai@virginia.edu; Fax: 434-982-5660

Authors

Shifeng Nian — Soft Biomatter Laboratory, Department of Materials Science and Engineering, University of Virginia, Charlottesville, Virginia 22904, United States; orcid.org/0000-0002-2243-6329

Baiqiang Huang — Soft Biomatter Laboratory, Department of Materials Science and Engineering, University of Virginia, Charlottesville, Virginia 22904, United States

Guillaume Freychet – National Synchrotron Light Source-II, Brookhaven National Laboratory, Upton, New York 11973, United States

Mikhail Zhernenkov — National Synchrotron Light Source-II, Brookhaven National Laboratory, Upton, New York 11973, United States; occid.org/0000-0003-3604-0672

Complete contact information is available at: https://pubs.acs.org/10.1021/acs.macromol.2c02053

Author Contributions

S.N. and B.H. provided equal contribution. L.H.C., S.N., and B.H. designed the research. S.N. and B.H. synthesized the polymers and performed WAXS measurements and analysis. G.F. and M.Z. helped with WAXS measurements and data analysis. L.H.C. analyzed the data, developed the theory, and wrote the paper. All authors reviewed and commented on the paper. L.H.C. conceived and supervised the study.

Notes

The authors declare the following competing financial interest(s): L.H.C. and S.N. have filed a U.S. provisional patent application (No. 63/395,430) for the synthesis and applications of foldable bottlebrush polymers.

ACKNOWLEDGMENTS

We thank Dr. Ting Ge for helpful discussion and Zihao Gong for help with initial polymer synthesis. L.H.C. acknowledges the support from NSF (CAREER DMR-1944625) and ACS Petroleum Research Fund (PRF) (6132047-DNI). This research used the SMI beamline (12-ID) of the National Synchrotron Light Source II, a U.S. Department of Energy (DOE) Office of Science User Facility operated for the DOE Office of Science by Brookhaven National Laboratory under contract no. DE-SC0012704.

REFERENCES

- (1) Chandran, P. L.; Horkay, F. Aggrecan, an Unusual Polyelectrolyte: Review of Solution Behavior and Physiological Implications. *Acta Biomater.* **2012**, *8*, 3–12.
- (2) Papagiannopoulos, A.; Waigh, T. A.; Hardingham, T.; Heinrich, M. Solution Structure and Dynamics of Cartilage Aggrecan. *Biomacromolecules* **2006**, *7*, 2162–2172.
- (3) Horkay, F.; Chremos, A.; Douglas, J. F.; Jones, R.; Lou, J.; Xia, Y. Comparative Experimental and Computational Study of Synthetic and

- Natural Bottlebrush Polyelectrolyte Solutions. J. Chem. Phys. 2021, 155, 074901.
- (4) McCutchen, C. W. The Frictional Properties of Animal Joints. *Wear* **1962**, *5*, 1–17.
- (5) Zappone, B.; Ruths, M.; Greene, G. W.; Jay, G. D.; Israelachvili, J. N. Adsorption, Lubrication, and Wear of Lubricin on Model Surfaces: Polymer Brush-like Behavior of a Glycoprotein. *Biophys. J.* **2007**, *92*, 1693–1708.
- (6) Button, B.; Cai, L.-H.; Ehre, C.; Kesimer, M.; Hill, D. B.; Sheehan, J. K.; Boucher, R. C.; Rubinstein, M. A Periciliary Brush Promotes the Lung Health by Separating the Mucus Layer from Airway Epithelia. *Science* **2012**, *337*, 937–941.
- (7) Roy, M. G.; Livraghi-Butrico, A.; Fletcher, A. A.; McElwee, M. M.; Evans, S. E.; Boerner, R. M.; Alexander, S. N.; Bellinghausen, L. K.; Song, A. S.; Petrova, Y. M.; et al. MucSb Is Required for Airway Defence. *Nature* **2014**, *505*, 412–416.
- (8) Paszek, M. J.; DuFort, C. C.; Rossier, O.; Bainer, R.; Mouw, J. K.; Godula, K.; Hudak, J. E.; Lakins, J. N.; Wijekoon, A. C.; Cassereau, L.; et al. The Cancer Glycocalyx Mechanically Primes Integrin-Mediated Growth and Survival. *Nature* **2014**, *511*, 319–325.
- (9) Sheiko, S. S.; Sumerlin, B. S.; Matyjaszewski, K. Cylindrical Molecular Brushes: Synthesis, Characterization, and Properties. *Prog. Polym. Sci.* **2008**, *33*, 759–785.
- (10) Li, Z.; Tang, M.; Liang, S.; Zhang, M.; Biesold, G. M.; He, Y.; Hao, S. M.; Choi, W.; Liu, Y.; Peng, J.; et al. Bottlebrush Polymers: From Controlled Synthesis, Self-Assembly, Properties to Applications. *Prog. Polym. Sci.* **2021**, *116*, 101387.
- (11) Johnson, J. A.; Lu, Y. Y.; Burts, A. O.; Xia, Y.; Durrell, A. C.; Tirrell, D. A.; Grubbs, R. H. Drug-Loaded, Bivalent-Bottle-Brush Polymers by Graft-through ROMP. *Macromolecules* **2010**, *43*, 10326–10335.
- (12) Sowers, M. A.; McCombs, J. R.; Wang, Y.; Paletta, J. T.; Morton, S. W.; Dreaden, E. C.; Boska, M. D.; Ottaviani, M.; Hammond, P. T.; Rajca, A.; et al. Redox-Responsive Branched-Bottlebrush Polymers for in Vivo MRI and Fluorescence Imaging. *Nat. Commun.* **2014**, *5*, 5460.
- (13) Guo, Z. H.; Le, A. N.; Feng, X.; Choo, Y.; Liu, B.; Wang, D.; Wan, Z.; Gu, Y.; Zhao, J.; Li, V.; et al. Janus Graft Block Copolymers: Design of a Polymer Architecture for Independently Tuned Nanostructures and Polymer Properties. *Angew. Chem., Int. Ed.* **2018**, *57*, 8493–8497.
- (14) Rokhlenko, Y.; Kawamoto, K.; Johnson, J. A.; Osuji, C. O. Sub-10 Nm Self-Assembly of Mesogen-Containing Grafted Macromonomers and Their Bottlebrush Polymers. *Macromolecules* **2018**, 51, 3680–3690.
- (15) Yamauchi, Y.; Horimoto, N. N.; Yamada, K.; Matsushita, Y.; Takeuchi, M.; Ishida, Y. Two-Step Divergent Synthesis of Monodisperse and Ultra-Long Bottlebrush Polymers from an Easily Purifiable ROMP Monomer. *Angew. Chem., Int. Ed.* **2021**, *60*, 1528–1534
- (16) Neugebauer, D.; Zhang, Y.; Pakula, T.; Sheiko, S. S.; Matyjaszewski, K. Densely-Grafted and Double-Grafted PEO Brushes via ATRP. A Route to Soft Elastomers. *Macromolecules* **2003**, *36*, 6746–6755.
- (17) Hu, M.; Xia, Y.; McKenna, G. B.; Kornfield, J. A.; Grubbs, R. H. Linear Rheological Response of a Series of Densely Branched Brush Polymers. *Macromolecules* **2011**, *44*, 6935–6943.
- (18) Abbasi, M.; Faust, L.; Wilhelm, M. Comb and Bottlebrush Polymers with Superior Rheological and Mechanical Properties. *Adv. Mater.* **2019**, *31*, 1806484.
- (19) Vatankhah-Varnoosfaderani, M.; Daniel, W. F. M. M.; Zhushma, A. P.; Li, Q.; Morgan, B. J.; Matyjaszewski, K.; Armstrong, D. P.; Spontak, R. J.; Dobrynin, A. V.; Sheiko, S. S. Bottlebrush Elastomers: A New Platform for Freestanding Electroactuation. *Adv. Mater.* **2017**, *29*, 1604209.
- (20) Yavitt, B. M.; Gai, Y.; Song, D. P.; Winter, H. H.; Watkins, J. J. High Molecular Mobility and Viscoelasticity of Microphase-Separated Bottlebrush Diblock Copolymer Melts. *Macromolecules* **2017**, *50*, 396–405.

- (21) López-Barrón, C. R.; Brant, P.; Eberle, A. P. R.; Crowther, D. J. Linear Rheology and Structure of Molecular Bottlebrushes with Short Side Chains. *J. Rheol* **2015**, *59*, 865–883.
- (22) Dalsin, S. J.; Hillmyer, M. A.; Bates, F. S. Linear Rheology of Polyolefin-Based Bottlebrush Polymers. *Macromolecules* **2015**, *48*, 4680–4691.
- (23) Banquy, X.; Burdyńska, J.; Lee, D. W.; Matyjaszewski, K.; Israelachvili, J. Bioinspired Bottle-Brush Polymer Exhibits Low Friction and Amontons-like Behavior. *J. Am. Chem. Soc.* **2014**, *136*, 6199–6202.
- (24) Arrington, K. J.; Radzinski, S. C.; Drummey, K. J.; Long, T. E.; Matson, J. B. Reversibly Cross-Linkable Bottlebrush Polymers as Pressure-Sensitive Adhesives. *ACS Appl. Mater. Interfaces* **2018**, *10*, 26662–26668.
- (25) Sveinbjörnsson, B. R.; Weitekamp, R. A.; Miyake, G. M.; Xia, Y.; Atwater, H. A.; Grubbs, R. H. Rapid Self-Assembly of Brush Block Copolymers to Photonic Crystals. *Proc. Natl. Acad. Sci. U.S.A.* **2012**, 109, 14332–14336.
- (26) Daniel, W. F. M. M.; Burdyńska, J.; Vatankhah-Varnoosfaderani, M.; Matyjaszewski, K.; Paturej, J.; Rubinstein, M.; Dobrynin, A. V.; Sheiko, S. S. Solvent-Free, Supersoft and Superelastic Bottlebrush Melts and Networks. *Nat. Mater.* **2016**, *15*, 183–189.
- (27) Cai, L.-H.; Kodger, T. E.; Guerra, R. E.; Pegoraro, A. F.; Rubinstein, M.; Weitz, D. A. Soft Poly(Dimethylsiloxane) Elastomers from Architecture-Driven Entanglement Free Design. *Adv. Mater.* **2015**, *27*, 5132–5140.
- (28) Vatankhah-Varnosfaderani, M.; Keith, A. N.; Cong, Y.; Liang, H.; Rosenthal, M.; Sztucki, M.; Clair, C.; Magonov, S.; Ivanov, D. A.; Dobrynin, A. V.; et al. Chameleon-like Elastomers with Molecularly Encoded Strain-Adaptive Stiffening and Coloration. *Science* **2018**, *359*, 1509–1513.
- (29) Nian, S.; Lian, H.; Gong, Z.; Zhernenkov, M.; Qin, J.; Cai, L.-H. Molecular Architecture Directs Linear-Bottlebrush-Linear Triblock Copolymers to Self-Assemble to Soft Reprocessable Elastomers. ACS Macro Lett. 2019, 8, 1528–1534.
- (30) Nian, S.; Zhu, J.; Zhang, H.; Gong, Z.; Freychet, G.; Zhernenkov, M.; Xu, B.; Cai, L. H. Three-Dimensional Printable, Extremely Soft, Stretchable, and Reversible Elastomers from Molecular Architecture-Directed Assembly. *Chem. Mater.* **2021**, 33, 2436–2445.
- (31) Cai, L.-H. Molecular Understanding for Large Deformations of Soft Bottlebrush Polymer Networks. *Soft Matter* **2020**, *16*, 6259–6264
- (32) Nian, S.; Fan, Z.; Freychet, G.; Zhernenkov, M.; Redemann, S.; Cai, L. H. Self-Assembly of Flexible Linear-Semiflexible Bottlebrush-Flexible Linear Triblock Copolymers. *Macromolecules* **2021**, *54*, 9361–9371
- (33) Chen, C.; Fei, H.-F.; Watkins, J. J.; Crosby, A. J. Soft Double-Network Polydimethylsiloxane: Fast Healing of Fracture Toughness. *J. Mater. Chem. A* **2022**, *10*, 11667–11675.
- (34) Chremos, A.; Douglas, J. F. A Comparative Study of Thermodynamic, Conformational, and Structural Properties of Bottlebrush with Star and Ring Polymer Melts. *J. Chem. Phys.* **2018**, 149, 044904.
- (35) Liang, H.; Wang, Z.; Dobrynin, A. V. Scattering from Melts of Combs and Bottlebrushes: Molecular Dynamics Simulations and Theoretical Study. *Macromolecules* **2019**, *52*, 5555–5562.
- (36) Sarapas, J. M.; Martin, T. B.; Chremos, A.; Douglas, J. F.; Beers, K. L. Bottlebrush Polymers in the Melt and Polyelectrolytes in Solution Share Common Structural Features. *Proc. Natl. Acad. Sci. U.S.A.* **2020**, *117*, 5168–5175.
- (37) Paturej, J. J.; Sheiko, S. S.; Panyukov, S.; Rubinstein, M. Molecular Structure of Bottlebrush Polymers in Melts. *Sci. Adv.* **2016**, 2, No. e1601478.
- (38) Chan, J. M.; Kordon, A. C.; Zhang, R.; Wang, M. Direct Visualization of Bottlebrush Polymer Conformations in the Solid State. *Proc. Natl. Acad. Sci. U.S.A.* **2021**, *118*, No. e2109534118.
- (39) López-Barrón, C. R.; Tsou, A. H.; Younker, J. M.; Norman, A. I.; Schaefer, J. J.; Hagadorn, J. R.; Throckmorton, J. A. Microstructure

- of Crystallizable α -Olefin Molecular Bottlebrushes: Isotactic and Atactic Poly(1-octadecene). *Macromolecules* **2018**, *51*, 872–883.
- (40) Liberman, L.; Coughlin, M. L.; Weigand, S.; Edmund, J.; Bates, F. S.; Lodge, T. P. Impact of Side-Chain Length on the Self-Assembly of Linear-Bottlebrush Diblock Copolymers. *Macromolecules* **2022**, *55*, 4947–4955.
- (41) Nian, S.; Cai, L.-H. Dynamic Mechanical Properties of Self-Assembled Bottlebrush Polymer Networks. *Macromolecules* **2022**, *55*, 8058–8066.
- (42) Matyjaszewski, K.; Jakubowski, W.; Min, K.; Tang, W.; Huang, J.; Braunecker, W. A.; Tsarevsky, N. V. Diminishing Catalyst Concentration in Atom Transfer Radical Polymerization with Reducing Agents. *Proc. Natl. Acad. Sci. U.S.A.* **2006**, *103*, 15309–15314.
- (43) Luo, Y.; Montarnal, D.; Kim, S.; Shi, W.; Barteau, K. P.; Pester, C. W.; Hustad, P. D.; Christianson, M. D.; Fredrickson, G. H.; Kramer, E. J.; et al. Poly(Dimethylsiloxane-b-Methyl Methacrylate): A Promising Candidate for Sub-10 Nm Patterning. *Macromolecules* **2015**, *48*, 3422–3430.
- (44) Cai, L.-H.; Panyukov, S.; Rubinstein, M. Mobility of Nonsticky Nanoparticles in Polymer Liquids. *Macromolecules* **2011**, 44, 7853–7863.
- (45) Cai, L.-H.; Panyukov, S.; Rubinstein, M. Hopping Diffusion of Nanoparticles in Polymer Matrices. *Macromolecules* **2015**, *48*, 847–862.
- (46) Wang, Z.; Zheng, X.; Ouchi, T.; Kouznetsova, T. B.; Beech, H. K.; Av-Ron, S.; Matsuda, T.; Bowser, B. H.; Wang, S.; Johnson, J. A.; et al. Toughening Hydrogels through Force-Triggered Chemical Reactions That Lengthen Polymer Strands. *Science* **2021**, *374*, 193.
- (47) Nian, S.; Patil, S.; Zhang, S.; Kim, M.; Chen, Q.; Zhernenkov, M.; Ge, T.; Cheng, S.; Cai, L.Dynamics of Associative Polymers with High Density of Reversible Bonds. **2022**, arXiv:2206.14036.
- (48) Wu, J.; Cai, L.-H.; Weitz, D. A. Tough Self-Healing Elastomers by Molecular Enforced Integration of Covalent and Reversible Networks. *Adv. Mater.* **2017**, *29*, 1702616.
- (49) Stukalin, E. B.; Cai, L.-H.; Kumar, N. A.; Leibler, L.; Rubinstein, M. Self-Healing of Unentangled Polymer Networks with Reversible Bonds. *Macromolecules* **2013**, *46*, 7525–7541.
- (50) Zhu, J.; Cai, L.-H. All-Aqueous Printing of Viscoelastic Droplets in Yield-Stress Fluids. *Acta Biomater.* **2022**, DOI: 10.1016/j.actbio.2022.09.031.
- (51) Zhu, J.; He, Y.; Kong, L.; He, Z.; Kang, K. Y.; Grady, S. P.; Nguyen, L. Q.; Chen, D.; Wang, Y.; Oberholzer, J.; et al. Digital Assembly of Spherical Viscoelastic Bio-Ink Particles. *Adv. Funct. Mater.* **2022**, 32, 2109004.